 doi:10.20944/preprints202208.0028.v1

Article

Depolarizing Effects in Hydrogen Bond Energy in 3_{10}-Helices Revealed by Quantum Chemical Analysis

Hiroko X. Kondo[1,2,3,*], Haruki Nakamura[4] and Yu Takano[2,4,*]

[1] School of Regional Innovation and Social Design Engineering, Faculty of Engineering, Kitami Institute of Technology, Kitami, Hokkaido 090-8507, Japan
[2] Department of Biomedical Information Sciences, Graduate School of Information Sciences, Hiroshima City University, Hiroshima 731-3194, Japan
[3] Laboratory for Computational Molecular Design, RIKEN Center for Biosystems Dynamics Research, 6-2-3, Furuedai, Suita, 565-0874, Japan
[4] Institute for Protein Research, Osaka University, Suita 565-0871, Japan
* Correspondence: h_kondo@mail.kitami-it.ac.jp; Tel.: +81-157-26-9401 (H.X.K), ytakano@hiroshima-cu.ac.jp; Tel.: +81-082-830-1825 (Y.T)

Abstract: Hydrogen-bond (H-bond) energies in 3_{10}-helices of short alanine peptides were systematically examined by precise DFT calculations with the negative fragmentation approach (NFA), a modified method based on the molecular tailoring approach. The contribution of each H-bond was evaluated in detail from the 3_{10}-helical conformation of total energies (whole helical model; $WH_{3\text{-}10}$ model), and the results were compared with the property of H-bond in α-helix from our previous study. The H-bond energies of the $WH_{3\text{-}10}$ model exhibited tendencies different from those exhibited by the α-helix, in that they depended on the helical position of the relevant H-bond pair. H-bond pairs adjacent to the terminal H-bond pairs were observed to be strongly destabilized. The analysis of electronic structures indicated that structural characteristics cause the destabilization of the H-bond in 3_{10}-helices. We also found that the longer the helix length, the more stable the H-bond in the terminal pairs of the $WH_{3\text{-}10}$ model, suggesting the action of H-bond cooperativity.

Keywords: 3_{10}-helix; hydrogen bond energy; density functional theory; negative fragmentation analysis

1. Introduction

Proteins are macromolecules essential for sustaining life and are also known to perform diverse biochemical functions in nature, such as molecular recognition, chemical catalysis, molecular switching, and the structural maintenance of cells[1–4]. They typically comprise 20 amino acids linked by peptide bonds. In aqueous solutions, the polypeptide chains in proteins fold according to their amino acid sequencing and form a three-dimensional structure. The remarkable functional versatility of proteins results from the chemical diversity of the side chains of the constituent amino acids, flexibility of the polypeptide chains, and excellent variety of structures rendered possible by the wide range of potential amino acid sequences.

Approximately 90% of the amino acid residues in protein structures are found in locally ordered secondary structures, such as an α-helix or a β-sheet[5]. These secondary structures assemble and fold to form three-dimensional structures, also known as tertiary structures. In other words, secondary structures are the building blocks of protein structures.

The helix is the most commonly observed secondary structure and can be classified into different helical conformations[3,4]. Of these, the α-helix is predominant and is found in 80% of all proteins[6]. The α-helix comprises a remarkably rigid arrangement of polypeptide chains and is a common secondary structural element in fibrous and globular proteins. It is arranged such that the peptide C=O group of the n-th residue along the helix

 doi:10.20944/preprints202208.0028.v1

faces the peptide N–H group of the (n + 4)-th residue, which results in the formation of a hydrogen bond with an N-to-O distance of ~2.8 Å. The second most common helical structure is the 3_{10}-helix, which is present in 20% of the helical structures[6]. This helix comprises three amino acid residues per helical turn, and a hydrogen bond is formed between the n-th and (n + 3)-th residues, resulting in a tighter packing of the backbone compared with the α-helix. This packing also forces the hydrogen bond to move outward from the helical axis.

Hydrogen bonds (H-bonds) play an essential role in secondary structure formation. Therefore, an accurate and quantitative evaluation of H-bonds is necessary to understand the principles of tertiary structure formation in proteins. It is well known that individual force fields used in classical molecular dynamics (MD) simulations exhibit the specific tendency of generating an α-helix or a β-strand[7–9]. Yoda et al. used MD simulations with explicit water molecules to compare the secondary structural properties of commonly used force fields[10,11]. They found that MD simulations using AMBER ff94[12] and ff99[13] were in remarkable agreement with experimental data for α-helical polypeptides but not for β-hairpin polypeptides. This preference of force fields on the secondary structure formation is typically not a problem in the MD simulations of rigid globular protein structures. However, it has become a critical issue in understanding functionally critical conformational changes[14–17] in the folding simulations of flexible disordered regions[14,15] and long loops between secondary structures[16,17]. Numerous attempts have been made to overcome this problem, such as increasing the torsional energies, rearrangements[18–21], and developing polarized charge models[22,23]. Regardless, the reasons behind the use of these methods remain unclear, and elucidation requires understanding the energy of hydrogen bonding in the secondary structure.

Several computational chemists have studied hydrogen bonding interactions in secondary structures at various levels of theoretical depth. Wieczorek and Dannenberg investigated H-bond cooperativity and the energetics of α-helices and suggested that various factors contribute to their stability[24,25]. Morozov et al. evaluated the origin of cooperativity in forming α-helices[26]. Zhao and Wu studied the role of cooperativity in the formation of α-helices by performing theoretical calculations on α-helix models constructed using a simple repeating unit method[27]. Parthasarathi et al. studied H-bond interactions in an α-helix model using the atom-in-molecules method[28]. Ismer et al. investigated the temperature dependence of the stability of α-, π-, and 3_{10}-helices comparing with a fully extended structure using density functional theory and harmonic approximation[29].

In our previous study[30], we calculated the conformational energies of secondary structures formed by alanine oligopeptides using several quantum mechanical (QM) methods; these included the Hartree–Fock (HF) method, second-order Møller–Plesset perturbation theory (MP2), density functional theory (DFT), and molecular mechanics (MM) calculations with classical force-field AMBER ff99SB. The results showed that classical force fields can be used to approximate the energies of parallel and antiparallel β-sheets, which are provided by the QM method. However, the energies of the α-helical structures by the MM method were found to be significantly different from those given by the QM method. This difference might be attributable to the electrostatic energy associated with hydrogen bonding[30]. We also used a slightly modified version of the molecular tailoring approach (MTA)[31] in combination with DFT and MM calculations to resolve the individual interaction energies associated with each hydrogen bond formed in typical α-helices of different peptide lengths. We concluded that the H-bond energies of the α-helix are generally higher than those of separated H-bonds because of the depolarized electronic structures around the carbonyl oxygen and the participation of amide hydrogen in the H-bond. Such depolarizations redistribute the electron density and are caused by local short-ranged electrostatic interactions with neighboring species in the α-helical structure[32].

In the present study, we systematically investigated the H-bond energies and associated electron density changes in 3_{10}-helices using QM calculations and compared them with those observed for α-helices in our previous study[32]. The contribution of each H-

 doi:10.20944/preprints202208.0028.v1

bond was evaluated from the total conformational energy (whole-helical; $WH_{3\text{-}10}$ models). To understand the characteristics of the H-bond energy in 3_{10}-helices, we additionally evaluated the H-bond energies using the following simplified models: minimal hydrogen bond ($MH_{3\text{-}10}$) models, wherein only H-bond donors and acceptors were present with capping methyl groups, and the single tern ($ST_{3\text{-}10}$) model, which includes a single helical turn. The characteristic interactions essential for 3_{10}-helices were quantitatively discussed.

2. Materials and Methods

2.1. Whole-helical structure ($WH_{3\text{-}10}$), single-turn ($ST_{3\text{-}10}$), and minimal H-bond ($MH_{3\text{-}10}$) models

Whole-helical structure models of the 3_{10}-helices ($WH_{3\text{-}10}$) were constructed using oligoalanine peptides capped with the acetyl (Ace) and *N*-methyl amide groups (Nme), referred to as Ace-$(Ala)_n$-Nme. We used dipeptide-to-heptapeptide alanines (n = 2–7) for the $WH_{3\text{-}10}$ model, which consists of Ace-$(Ala)_n$-Nme, is denoted by $WH_{3\text{-}10}$-n. The backbone dihedral angles (φ, ψ) for each residue were set to $\varphi = -49°$ and $\psi = -26°$. For comparison, we used the previously reported whole-helical structure models of the α-helices (WH_{α}-n), composed of the alanine oligopeptide Ace-$(Ala)_n$-Nme (n = 3–8), with $\varphi = -57°$ and $\psi = -47°$[3]. These structures were optimized in the gas phase by the energy minimization of the electronic state while keeping the backbone dihedral angles fixed at the aforementioned values.

One-to-six H-bonds were present between the C=O and N–H groups in the backbone of the optimized $WH_{3\text{-}10}$ models, as H-bonds were formed between an i-th and (i + 3)-th peptide pair for $WH_{3\text{-}10}$ and between an i-th and (i + 4)-th peptide pair for WH_{α}. The s-th H-bond in Ace-$(Ala)_n$-Nme, counting from the N-terminus, is represented by n-s (Figure 1a shows $WH_{3\text{-}10}$-4 as an example). The H-bond energies were individually calculated using DFT, as described below.

To analyze the origin of the H-bond interaction energy in 3_{10}-helices, we designed two simplified models. One is an $ST_{3\text{-}10}$ model, composed of two successive alanine residues capped by Ace and Nme groups at the N- and C-termini, respectively (second column in Figure 1b). The other is an $MH_{3\text{-}10}$ model, which comprises two separated *N*-methyl acetamide molecules and mimics a single H-bond between the C=O and N–H groups in the backbone (third column in Figure 1b). The atomic positions of these two models were the same as those of the corresponding $WH_{3\text{-}10}$ models, except for the N- and C-terminal capping groups. The computation of the individual H-bond energies for these models was conducted in the same manner as that for each backbone H-bond in the $WH_{3\text{-}10}$ models, as described below. The H-bond energies of the three models were then compared.

Preprints (www.preprints.org) | NOT PEER-REVIEWED | Posted: 2 August 2022 doi:10.20944/preprints202208.0028.v1

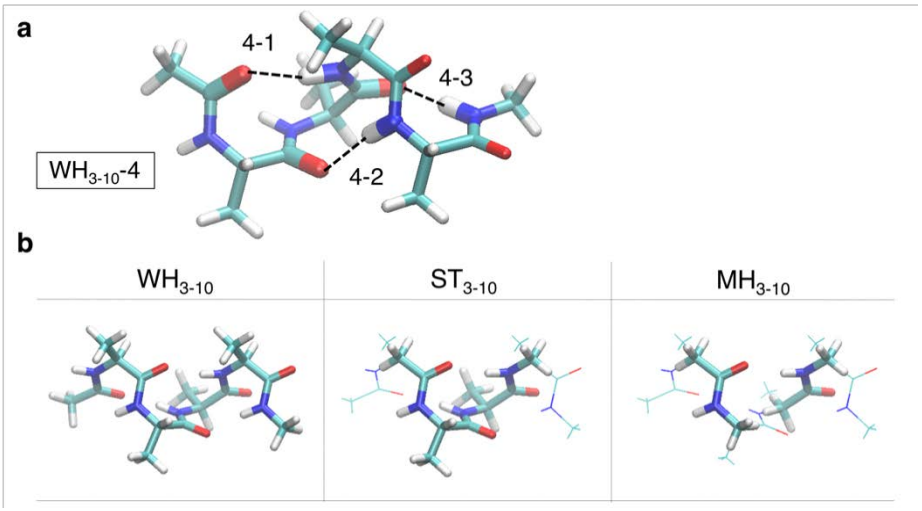

Figure 1. (a) Structure of the 3_{10}-helix composed of Ace-(Ala)$_4$-Nme (WH$_{3\text{-}10}$-4) with the notation of each H-bond in the structure. (b) Structures of the whole-helical (WH$_{3\text{-}10}$), single-turn (ST$_{3\text{-}10}$), and minimal H-bond (MH$_{3\text{-}10}$) models of WH$_{3\text{-}10}$-4, as examples.

2.2. Calculation of H-bond energies using the negative fragmentation approach

The extraction of the H-bond energy from the total energy of a large molecule wherein the donor and acceptor atoms are linked through several covalent bonds, such as in α- and 3_{10}-helices, is not straightforward. In this study, we systematically computed the backbone H-bond energies in the WH$_{3\text{-}10}$ models in the same manner as that computing the H-bond energies in the WH$_a$ models as reported previously[32], where we modified the MTA developed by Deshmukh et al.[31]. This method is denoted here as the negative fragmentation approach (NFA). In the NFA, the H-bond energy, E_{HB}, in Ace-(Ala)$_n$-Nme can be calculated using the following equation:

$$E_{\mathrm{HB}} = E_{\mathrm{sys}} - E_{\overline{\mathrm{A}}} - E_{\overline{\mathrm{D}}} + E_{\overline{\mathrm{AUD}}}, \quad (1)$$

where E_{sys}, $E_{\overline{\mathrm{A}}}$, $E_{\overline{\mathrm{D}}}$, and $E_{\overline{\mathrm{AUD}}}$ are the energies of the entire system, system lacking the acceptor group, system without the donor group, and system lacking both acceptor and donor groups, respectively; detailed descriptions are available in our previous study[32]. In the original MTA, the energy of the entire system was estimated using the energies of all fragments[31]. In the NFA, we used the total energy of the entire system and showed that the difference between the results was negligible[32].

The change in the electron density upon H-bond formation, $\Delta\rho_{\mathrm{HB}}$, was evaluated as follows:

$$\Delta\rho_{\mathrm{HB}} = \rho_{\mathrm{sys}} - \rho_{\overline{\mathrm{A}}} - \rho_{\overline{\mathrm{D}}} + \rho_{\overline{\mathrm{AUD}}}. \quad (2)$$

For comparison, we also computed the H-bond interaction energies via MM using the AMBER ff99SB force-field parameters[13], $E_{\mathrm{HB\_MM}}$, for the corresponding H-bonds, as follows:

$$E_{\mathrm{HB\_MM}} = \sum_{i\in I, j\in J} \frac{q_i q_j}{r_{ij}} + \sum_{i\in, j\in J} \left(\frac{B_{ij}}{r_{ij}^{12}} - \frac{C_{ij}}{r_{ij}^{6}}\right), \quad (3)$$

where I and J are the four atoms constituting the peptide group, namely, C, O, N, and H, of an acceptor and a donor involved in the H-bond, respectively. B_{ij} and C_{ij} are the Lennard–Jones coefficients, r_{ij} is the distance between the i-th and j-th atoms, and q_i is the partial atomic charge of the i-th atom. The MM energy was calculated for the WH$_{3\text{-}10}$ and MH$_{3\text{-}10}$ models.

Calculations for all models were performed using the Gaussian09 program package[33]. The B97D exchange–correlation functional was used with 6-31+G(d) basis sets.

Preprints (www.preprints.org) | NOT PEER-REVIEWED | Posted: 2 August 2022 doi:10.20944/preprints202208.0028.v1

This method is capable of correctly describing van der Waals interactions and is comparable with the MP2 method in the calculation of the H-bond interaction energies of the Ace–(Ala)$_n$-Nme system in the gas phase[30]. Changes in electron density were computed using cube files provided in the Gaussian09 program packages[33], and molecules that exhibited such changes were depicted using UCSF Chimera[34]. The other molecular structures were drawn using VMD software[35].

3. Results

3.1. Structures of H-bonds of the optimized whole-helical models of 3$_{10}$-helices

The H-bond distances and torsion angles were analyzed for the optimized WH$_{3\text{-}10}$ models. The H-bond distance was defined as the distance between the oxygen atom in the backbone C=O group and the hydrogen atom in the backbone N–H group, which form an H-bond. A histogram of the H-bond distances and a plot of the H-bond distances for each pair in the WH$_{3\text{-}10}$ and the corresponding α-helix models (WH$_a$) are shown in Figure 2. The mean values and standard deviations of the H-bond distances for the WH$_{3\text{-}10}$ and WH$_a$ models were found to be 2.05 ± 0.04 and 2.30 ± 0.07 Å, respectively. The WH$_{3\text{-}10}$ models generally exhibited shorter H-bonds than those exhibited by the WH$_a$ models. A characteristic feature of WH$_{3\text{-}10}$ is that the H-bond distances tend to be greater in the H-bond pairs adjacent to the terminal ones (Figure 2b and Table 1). The 4–2 H-bond pair in WH$_{3\text{-}10}$, sandwiched between the N- and C-terminal H-bond pairs (Figure 1a), showed the longest H-bond distance.

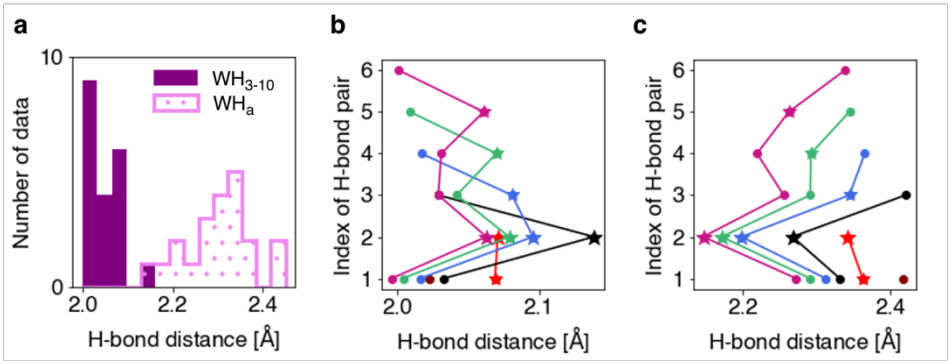

Figure 2. (a) Histograms of the H-bond distances in the WH$_{3\text{-}10}$ and WH$_a$ models. Plots of the H-bond distances in the (b) WH$_{3\text{-}10}$ and (c) WH$_a$ models of each length. The H-bond distances of Ace-(Ala)$_n$-Nme, which forms one-to-six H-bonds, are shown in maroon, red, black, blue, green, and violet–red, respectively. The star indicates the H-bond pairs adjacent to the terminal pair.

Table 1. Mean values and standard deviations of the H-bond distances, r_{OH}, of the WH$_{3\text{-}10}$ and WH$_a$ models.

	WH$_{3\text{-}10}$ †	WH$_a$
Terminal	2.02 ± 0.02	2.35 ± 0.04
Pairs adjacent to the terminal ‡	2.08 ± 0.03	2.26 ± 0.07
Others (inner)	2.03 ± 0.01	2.26 ± 0.03
All	2.05 ± 0.04	2.30 ± 0.07

† H-bond distance is shown in angstroms.
‡ 3-1 and 3-2 of WH$_{3\text{-}10}$-3 and 4-1 and 4-2 of WH$_a$-4 are included (they are also the terminal pairs).

The H-bond torsion angle was evaluated as the angle between the vectors of the C=O and N–H atoms on the backbone. This corresponds to the dihedral angle of the C, O, N, and H atoms comprising the H-bond. As shown in Figure 3b, the N-terminal H-bonding pairs in the WH$_a$ model exhibited significantly different torsion angles than those exhibited by the other H-bonding pairs. In the WH$_{3\text{-}10}$ models, the H-bond torsion angles of individual H-bond pairs varied with the length of the helix and their position in it (Figure

Preprints (www.preprints.org) | NOT PEER-REVIEWED | Posted: 2 August 2022 doi:10.20944/preprints202208.0028.v1

3a). In addition, the H-bond torsion angles of the $WH_{3\text{-}10}$ models are narrowly distributed, indicating that the molecular backbone of the $WH_{3\text{-}10}$ models imposes stronger structural constraints than those of the WH_a models. These constraints can possibly lead to considerably shorter H-bond distances in the $WH_{3\text{-}10}$ models than in the WH_a models as shown in Figure 2a.

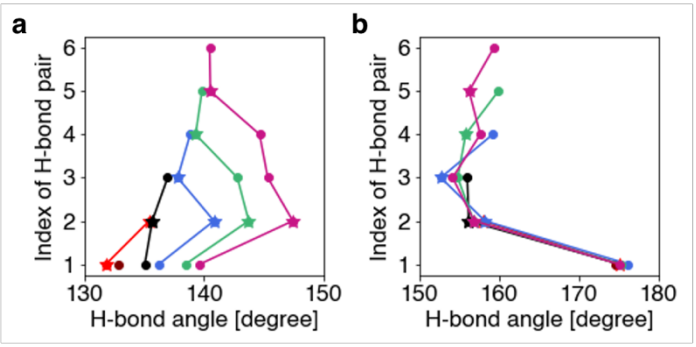

Figure 3. H-bond torsion angles of the (a) $WH_{3\text{-}10}$ and (b) WH_a models. H-bond torsion angles of Ace-$(Ala)_n$-Nme, which forms one-to-six H-bonds, are shown in maroon, red, black, blue, green, and violet–red, respectively. The torsion angles of the H-bond adjacent to the terminal H-bond pair are indicated by a star.

3.2. Comparison of H-bond energy in helical model systems

To investigate the effects of the helical backbone atoms linking the H-bond acceptor and donor on the H-bond energies, we compared the H-bond energies for the $WH_{3\text{-}10}$, $ST_{3\text{-}10}$, and $MH_{3\text{-}10}$ models of the 3_{10}-helices, as well as those for the α-helices from our previous study, namely WH_a, ST_a, and MH_a[32]. In the $MH_{3\text{-}10}$ and MH_a models, the two peptide groups of hydrogen donors and acceptors were separated without linking the helical backbone atoms. In Figure 4a, the H-bond energies of the $WH_{3\text{-}10}$ (black) and $ST_{3\text{-}10}$ (red) models are plotted versus those of the $MH_{3\text{-}10}$ models for the 3_{10}-helices. Those of the WH_a, ST_a, and MH_a models for α-helices[32] are also shown in Figure 4b.

In the α-helices, the ST_a model reproduced the H-bond energies of the WH_a model (Figure 4b), indicating that the adjacent residue destabilized the H-bond with respect to the MH_a model[32]. In the 3_{10}-helices, the $ST_{3\text{-}10}$ models also destabilized the H-bond with respect to the $MH_{3\text{-}10}$ models, similar to the α-helices, but failed to provide the equivalent H-bond energies. In particular, the H-bond pairs adjacent to the N- or C-terminus were strongly destabilized in energy (underlined in Table S1). This indicates that the helical backbone atoms participating in the H-bond are partly involved in the destabilization of the H-bond, but that other factors also lead to unstable H-bond energies. We also found a tendency that the longer the helix length, the more stable the H-bond energy of the N- and C-terminal pairs in the $WH_{3\text{-}10}$ model (shown in Table S1). However, there is an exception: the H-bond energies of the N- and C-terminal pairs in $WH_{3\text{-}10}$-3 were observed to be higher than those of $WH_{3\text{-}10}$-2. They are close to those of the H-bond pairs adjacent to the terminal H-bond pair in the other systems. This would be because the N- and C-termini are adjacent to each other in $WH_{3\text{-}10}$-3. For example, the N-terminal H-bond pair of $WH_{3\text{-}10}$-3, 3-1, is adjacent to the C-terminal H-bond pair 3-2, and vice versa.

Considering the H-bond energies of the $ST_{3\text{-}10}$ model, only the H-bond pairs next to the N- or C-terminal were destabilized by the adjacent residue, as shown in Figure 4a. The pair sandwiched between the N- and C-termini were also the most affected (4-2 of $WH_{3\text{-}10}$-4), which causes a difference in the linear regression coefficient between the $WH_{3\text{-}10}$ and $ST_{3\text{-}10}$ models, as shown in Figure 4a.

Preprints (www.preprints.org) | NOT PEER-REVIEWED | Posted: 2 August 2022 doi:10.20944/preprints202208.0028.v1

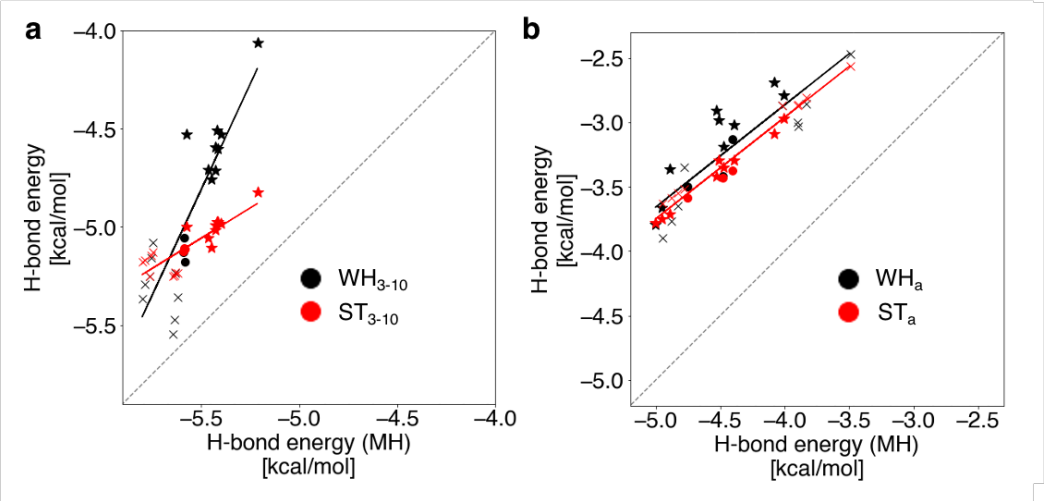

Figure 4. Correlations of the H-bond energies of the (a) WH (black) and ST (red) models versus those of the MH model in the 3_{10}-helices and (b) those in the α-helices[32]. The dashed line shows a guide where the longitudinal axis values have identical H-bond energies. The cross and star marks represent the H-bond pair of the terminal and that adjacent to the terminal, respectively.

To further examine the effect of neighboring residues on the H-bond energy of the 3_{10}-helices, we constructed additional models as follows: ST_{EC}, in which the $ST_{3\text{-}10}$ model, Ace-$(Ala)_2$-Nme, was extended to the C-terminal (Ace-$(Ala)_2$-Ala-Nme); ST_{EN}, in which the $ST_{3\text{-}10}$ model was extended to the N-terminal (Ace-Ala-$(Ala)_2$-Nme); ST_{ECN}, in which the $ST_{3\text{-}10}$ model was extended to both N- and C-termini (Ace-Ala-$(Ala)_2$-Ala-Nme); and ST_{E2N}, in which the $ST_{3\text{-}10}$ model was extended by two residues to the N-terminal (Ace-Ala-Ala-$(Ala)_2$-Nme). All peptide structures were generated based on the $WH_{3\text{-}10}$ model, and their H-bond energies were computed using the NFA.

As expected, in the ST_{ECN} model, both the N- and C-terminal H-bond pairs were adjacent to the target H-bond, thereby making the H-bond energy unstable (Figure 5). The ST_{EC} and ST_{EN} models were more stable than the ST_{ECN} models. The ST_{E2N} model showed nearly the same results as the $ST_{3\text{-}10}$ model, and higher energy values than those of the terminal pairs in the $WH_{3\text{-}10}$ model, as shown in the crosses in Figure 5.

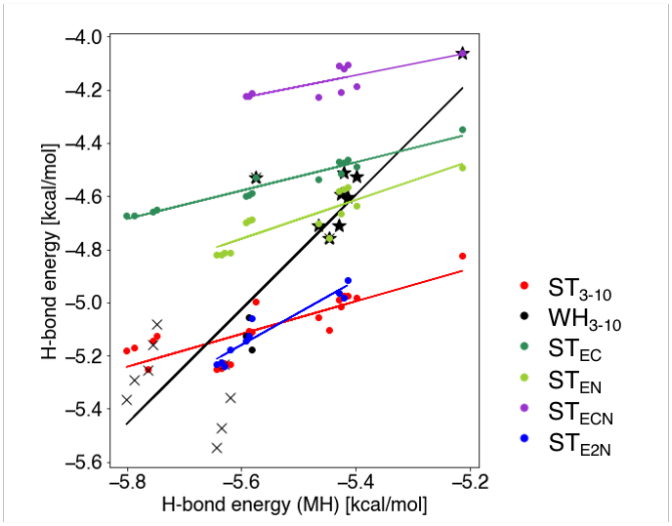

Figure 5. H-bond energies of the extended ST, $WH_{3\text{-}10}$, and $ST_{3\text{-}10}$ models versus those of the MH model. The cross and star marks of $WH_{3\text{-}10}$ represent the H-bond pair of the terminal and that adjacent to the terminal, respectively.

3.3. Electronic structures around the H-bond donors and acceptors

Preprints (www.preprints.org) | NOT PEER-REVIEWED | Posted: 2 August 2022 doi:10.20944/preprints202208.0028.v1

In addition to the H-bond energies, the NFA can approximately represent the change of electronic structures upon H-bond formation by Equation 2 in section 2.2. To examine the difference in the H-bond energy between the $WH_{3\text{-}10}$ and $ST_{3\text{-}10}$ models and the $ST_{3\text{-}10}$ and $MH_{3\text{-}10}$ models in the context of their electronic structures, the differences in the change in electron density were computed using Equations 4 and 5, respectively:

$$\Delta\Delta\rho_{HB}^{WH_{3\text{-}10}\text{-}ST_{3\text{-}10}} = \Delta\rho_{HB}^{WH_{3\text{-}10}} - \Delta\rho_{HB}^{ST_{3\text{-}10}}. \quad (4)$$

$$\Delta\Delta\rho_{HB}^{ST_{3\text{-}10}\text{-}MH_{3\text{-}10}} = \Delta\rho_{HB}^{ST_{3\text{-}10}} - \Delta\rho_{HB}^{MH_{3\text{-}10}}. \quad (5)$$

Figure 6 shows $\Delta\rho_{HB}^{WH_{3\text{-}10}}$ for the first and second H-bond pairs of $WH_{3\text{-}10}$-4 (4-1 and 4-2), in addition to both $\Delta\Delta\rho_{HB}^{WH_{3\text{-}10}-ST_{3\text{-}10}}$ and $\Delta\Delta\rho_{HB}^{ST_{3\text{-}10}\text{-}MH_{3\text{-}10}}$ for the same pairs. For $\Delta\rho_{HB}^{WH_{3\text{-}10}}$, we found that the electron density increases in the vicinity of the oxygen atom of the C=O group and that it decreases in the vicinity of the hydrogen atom of the N–H group, thus demonstrating the formation of the H-bond. The $\Delta\rho_{HB}^{WH_{3\text{-}10}}$ of 4-2 appears to be slightly smaller than that of 4-1, indicating a larger depolarization of 4-2 than 4-1. This larger depolarization results in a weaker H-bond at 4-2, as illustrated in Figures 6a and 6b. A remarkable difference was observed between 4-1 and 4-2: the $\Delta\Delta\rho_{HB}^{WH_{3\text{-}10}-ST_{3\text{-}10}}$ of 4-1 was considerably smaller than that of 4-2, implying that an effect other than the helical backbone atoms linking the H-bond pairs was at play in the 4-2 pair (Figures 6c and 6d). This could be the reason behind the difference in the H-bond energy between the $WH_{3\text{-}10}$ and $ST_{3\text{-}10}$ in the H-bond pairs adjacent to the terminal pairs. $\Delta\Delta\rho_{HB}^{ST_{3\text{-}10}\text{-}MH_{3\text{-}10}}$ indicates larger depolarization in the $ST_{3\text{-}10}$ model compared with the $MH_{3\text{-}10}$ model, as shown in Figures 6e and 6f.

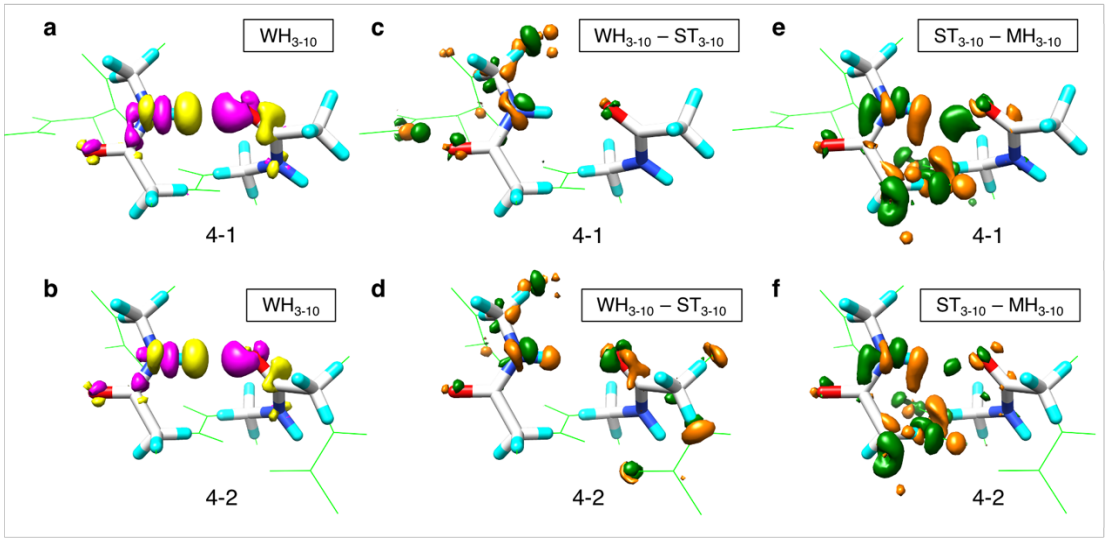

Figure 6. Electron density changes upon H-bond formation, $\Delta\rho_{HB}^{WH_{3\text{-}10}}$, for (a) 4-1 and (b) 4-2 in $WH_{3\text{-}10}$-4. The yellow surfaces represent the contour surfaces at −0.001 au, and the magenta ones are those at 0.001 au. The atoms in the whole $WH_{3\text{-}10}$ model are shown by green wire and those in the $MH_{3\text{-}10}$ models are shown using the stick model with CPK colors. The difference in the change in electron density between the $WH_{3\text{-}10}$ and $ST_{3\text{-}10}$ models, $\Delta\Delta\rho_{MTA}^{WH\text{–}ST_{3\text{-}10}}$, for (c) 4-1 and (d) 4-2 in $WH_{3\text{-}10}$-4. The dark-green surfaces represent the contour surfaces at –0.00015 au, and the orange ones are those at 0.00015 au. The difference in the change in electron density between the $ST_{3\text{-}10}$ and $MH_{3\text{-}10}$ models, $\Delta\Delta\rho_{MTA}^{ST\text{-}MH_{3\text{-}10}}$, for (e) 4-1 and (f) 4-2 in $WH_{3\text{-}10}$-4. The dark-green surfaces are the contour surfaces at –0.00015 au, and the orange ones are those at 0.00015 au.

3.4. Dependence of helix length on H-bond energies

We investigated the dependence of helix length on the mean value of the H-bond energies in the $WH_{3\text{-}10}$ and WH_a models. The mean H-bond energies of these models were plotted as functions of the minimum length of the corresponding helices, as shown in Figure 7. In WH_a models, the energy of the H-bond gradually stabilized with an increase

 doi:10.20944/preprints202208.0028.v1

in the length of the helix, demonstrating the well-known "H-bond cooperativity" phenomenon[24–27], where long-range interaction could make more stable helices. The mechanism behind the cooperativity in helix formation can be deconstructed into two parts, namely, electrostatic interactions between residues and nonadditive many-body effects caused by the redistribution of electron density with increasing helix length[26]. In the $WH_{3\text{-}10}$ model series, the H-bond of $ST_{3\text{-}10}$ was destabilized in the first increment of the minimum length of the helix, while subsequent increments gradually stabilized it. This is because the first increase in helix makes the H-bond adjacent to the terminal H-bond pair, leading to considerable destabilization of the H-bond, as discussed above. Subsequent elongation of the helix results in the stabilization of the terminal H-bond through H-bond cooperativity[25,27].

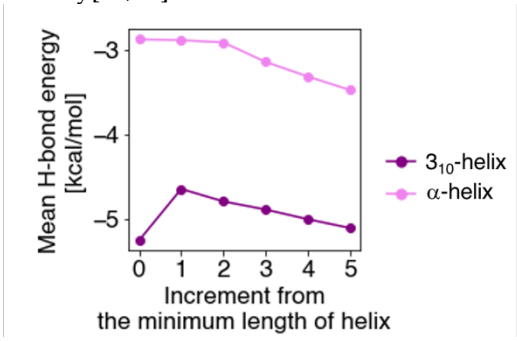

Figure 7. Mean H-bond energies plotted against increments of the minimum length of the helix in each helical model: n = 2 and 3 for the $WH_{3\text{-}10}$ and WH_{AH} models, respectively.

4. Discussion

We systematically investigated the H-bond energies of various 3_{10}-helices and found them to exhibit tendencies different from those exhibited by α-helices. Here, we discuss the following three issues: (i) why the H-bond energies in the $ST_{3\text{-}10}$ model are destabilized compared with those in the $MH_{3\text{-}10}$ model, (ii) why the H-bond pairs adjacent to the terminal pair are largely destabilized compared with other H-bond pairs, and (iii) why the terminal H-bond pairs are stabilized, particularly for long 3_{10}-helices.

For the issue (i), as mentioned in Section 3.3, the C=O and N–H groups participating in the H-bond were depolarized in the $ST_{3\text{-}10}$ model in comparison to the $MH_{3\text{-}10}$ model. This depolarization could be caused by the helical backbone atoms linking the H-bond pair (residue 2 of Figure 8). In α-helices, the adjacent C=O group is involved in depolarization[32]. However, in the 3_{10}-helices, the C=O group of the H-bond pair is closer to the adjacent N–H group (~2.8 Å), than to another adjacent C=O group (~3.4 Å). Therefore, the destabilization of the H-bond is attributed to the depolarization caused by the N–H group.

For the issue (ii), when $ST_{3\text{-}10}$ was extended to the N-terminus by a single residue (ST_{EN}), an additional H-bond was formed between the C=O group of residue -1 and the N–H group of residue 2. This H-bond formation causes polarization of the N–H group of residue 2, leading to further depolarization of the C=O group of residue -1. Thus, the H-bond could be destabilized. When ST_{EN} is extended to the N-terminal (ST_{E2N}), an additional H-bond is formed between the N=H group of residue 1 and C=O group of residue -2 (back side of the helix in the right panel of Figure 8). This H-bond formation induces polarization of the N–H group of residue 1, causing polarization of the adjacent C=O group of residue 0. This effect could cancel the depolarization effect by the N–H group of residue 2 on the C=O group of residue 0, thereby strengthening the H-bond. At the C-terminal, the similar depolarization effect could destabilize the H-bond.

For the issue (iii), H-bond cooperativity stabilizes the terminal H-bond pair indicated in Section 3.4, as well as α-helices[24–27].

Preprints (www.preprints.org) | NOT PEER-REVIEWED | Posted: 2 August 2022 doi:10.20944/preprints202208.0028.v1

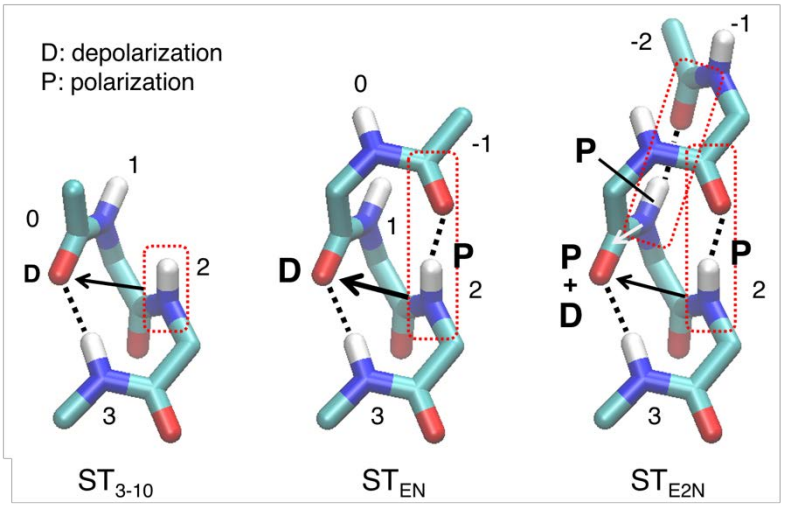

Figure 8. Schematic of the interactions between the H-bond acceptor and neighboring groups. The atoms of the model peptides ($ST_{3\text{-}10}$, ST_{EN}, and ST_{E2N} models of 7-3 in $WH_{3\text{-}10}$ as an example) are shown using the stick model. Hydrogen atoms, except for those in the N–H group, are not shown. The numbers in the figure represent the residue number.

The H-bond energies for the $WH_{3\text{-}10}$ and WH_a models were compared using QM (E_{HB} in Equation 1) and MM (E_{HB_MM} in Equation 3) calculations. Figure 9a exhibits the H-bond energies calculated with QM plotted versus those with MM for individual pairs of the $WH_{3\text{-}10}$ and WH_a models. In the WH_a models, the H-bond energies obtained via QM calculations were shown to be strongly correlated to those obtained via MM, with a correlation coefficient of 0.89. However, the MM calculations overestimated the magnitude of the H-bond energies by ~1 kcal/mol (the mean energy values obtained via QM and MM were -3.21 ± 0.39 and -4.24 ± 0.45 kcal/mol, respectively). Our previous study, wherein the energies were obtained via QM calculation, showed that the destabilization of the H-bond energies in the WH_a model was attributed to the depolarization of the H-bond donors and acceptors caused by adjacent residues[32].

In contrast, the H-bond energies for the $WH_{3\text{-}10}$ models obtained via QM calculation seem to be closer to those obtained with MM, and were more stable than those of the WH_a models (the mean energy values obtained via QM and MM for the $WH_{3\text{-}10}$ model were -4.96 ± 0.39 and -4.95 ± 0.24 kcal/mol, respectively). Unlike the WH_a models, the correlation between the QM and MM calculations was weak: the correlation coefficient was evaluated to be 0.54, as shown in Figure 9a.

In Figure 9b, the H-bond energies calculated with QM are plotted versus those with MM for individual pairs of the $MH_{3\text{-}10}$ models and MH_a models. Although the H-bond energies obtained via QM and MM for the MH_a models almost coincided[32], the H-bond energies obtained by QM were significantly more stable than those obtained via MM for the $MH_{3\text{-}10}$ models. However, unlike the $WH_{3\text{-}10}$ models, the correlation between the H-bond energies obtained via QM and MM for the $MH_{3\text{-}10}$ models was acceptable, a correlation coefficient was 0.88. The reason why the H-bond energies obtained using MM largely deviate from those obtained via QM may be the poor quality of the atomic partial charges in equation 3. Here, we used the AMBER ff99SB force-field parameters[13] for the atomic partial charges, which were originally determined by multiple-conformation models fitting to the local conformations of a single amino acid for both the α-helical and extended structures[36]. Thus, the parameters may well reproduce H-bond energies for the α-helical conformations MH_a, but not for the 3_{10}-helices $MH_{3\text{-}10}$.

Preprints (www.preprints.org) | NOT PEER-REVIEWED | Posted: 2 August 2022 doi:10.20944/preprints202208.0028.v1

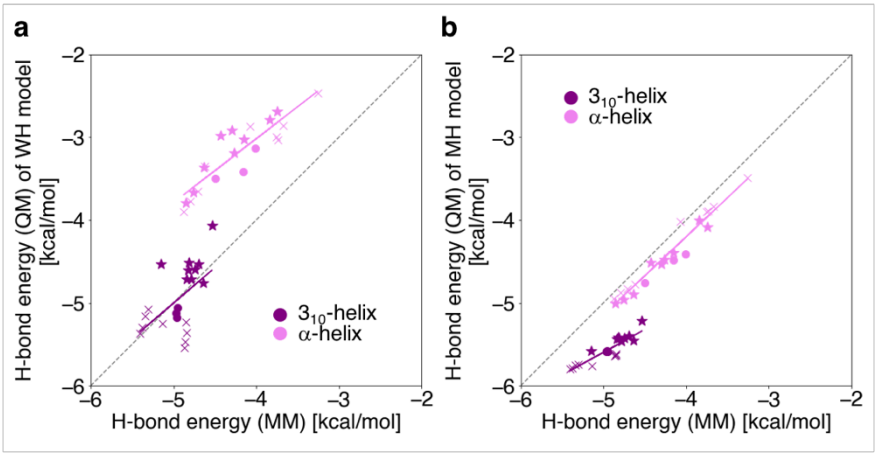

Figure 9. Correlations between the H-bond energies of the (a) WH models and the (b) MH models, calculated by the QM and MM methods for the 3_{10}-helices (purple) and α-helices (violet). The dashed line shows a guide where the H-bond energies of the longitudinal axis values and the MM calculations are identical. .

In the current study, it is revealed that the H-bond energy of 3_{10}-helix largely depends on its local conformation yielding the depolarization and on the long-ranged cooperativity effect. Those QM effects have not been included in the MM computations as well as for the H-bond energy of α-helix[32]. In order to improve the MM force fields, there could be two approaches: (i) by modifying the atomic partial charges, which are not constant values but depend on the atomic conformation, and (ii) by creating new backbone dihedral parameters, which depends on not only a single amino acid residue but also on the parameter set including the neighboring residues, as suggested by our previous paper[32].

5. Conclusions

In this study, the H-bond energies and associated changes in the electron density of the atoms forming H-bond of the 3_{10}-helices were systematically analyzed using the NFA method with high-quality DFT and MM computations and were compared with those of the α-helices. We prepared optimized structures of Ace-$(Ala)_n$-Nme, where n ranged from 2 to 7 for the whole-helical structure models ($WH_{3\text{-}10}$). To quantitatively investigate the origin of the H-bond energy in each helical model, we also constructed single-turn models ($ST_{3\text{-}10}$), which comprised two successive alanine residues capped by Ace and Nme groups at the N- and C-termini, respectively, and minimum H-bond models ($MH_{3\text{-}10}$), which comprised only pairs of Ace-Nme forming a single H-bond. The structures of the $ST_{3\text{-}10}$ and $MH_{3\text{-}10}$ models were based on the $WH_{3\text{-}10}$ model. The individual H-bond energies were then computed using the NFA.

The distribution of the H-bond distance of the $WH_{3\text{-}10}$ models was narrow, and these models exhibited lower values than those exhibited by the α-helical models (WH_a). The shorter H-bond distance observed in the $WH_{3\text{-}10}$ model was due to restrictions imposed by the tight helical structure. The H-bond energy of the $WH_{3\text{-}10}$ model exhibited a tendency different from those exhibited by the $ST_{3\text{-}10}$ and $MH_{3\text{-}10}$ models; it depended on the location of the H-bond pair in the 3_{10}-helices. Furthermore, the H-bonds in this model tended to be destabilized in the H-bond pairs adjacent to the terminal pairs and were stabilized at the terminal H-bond pairs. An analysis of changes in the electron density between the $WH_{3\text{-}10}$ and $ST_{3\text{-}10}$ models and between the $ST_{3\text{-}10}$ and $MH_{3\text{-}10}$ models suggested that the destabilization of the H-bond in the $ST_{3\text{-}10}$ model was attributed to the depolarization caused by the adjacent N–H group. It also suggested that the H-bond formation at this group causes polarization, leading to further depolarization of the C=O group participating in the H-bond pair and larger destabilization of the H-bond adjacent to the terminal H-bond pair.

Except for the first increment, elongation of the helix of the $WH_{3\text{-}10}$ model resulted in the stabilization of the terminal H-bond through H-bond cooperativity.

Supplementary Materials: The following supporting information can be downloaded from www.mdpi.com/xxx/s1, Table S1: H-bond energies of each H-bond pair.

Author Contributions: Conceptualization: Y.T. and H.N.; methodology: Y.T. and H.X.K.; software: H.X.K.; validation: H.X.K. and Y.T.; formal analysis: H.X.K. and Y.T.; investigation: H.X.K. and Y.T.; resources: Y.T. and H.X.K.; data curation: H.X.K. and Y.T.; writing—original draft preparation: H.X.K., Y.T., and H.N.; writing—review and editing: H.X.K., Y.T., and H.N.; visualization: H.X.K. and Y.T.; supervision: Y.T. and H.N.; project administration: Y.T.; funding acquisition: Y.T. All authors have read and agreed on the published version of the manuscript.

Funding: This work was funded by JSPS Grant-in-Aid for Scientific Research (C), 19K06589 and 22K06164, by MEXT Grant-in-Aid for Scientific Research on Transformative Research Areas (A) "Hyper-Ordered Structures Science," 20H05883, by JSPS Grants-in-Aid for Exploratory Research (23657103). The APC was funded by a JSPS Grant-in-Aid for Scientific Research (C), 22K06164.

Institutional Review Board Statement: Not applicable.

Informed Consent Statement: Not applicable.

Data Availability Statement: Not applicable.

Acknowledgments: The computations were performed at the Research Center for Computational Science, Okazaki, Japan (22-IMS-C007) and the RIKEN Advanced Center for Computing and Communication (ACCC). This study was performed in part under the Cooperative Research Program of the Institute for Protein Research, Osaka University, CR-18-02, CR-19-02, CR-20-02, CR-21-02, and CR-22-02.

Conflicts of Interest: The authors declare no conflicts of interest.

References

1. Jeffrey, G. A. *An Introduction to Hydrogen Bonding*; Oxford University Press, 1997.
2. Branden, C. I.; Tooze, J. *Introduction to Protein Structure*; Garland Science: New York, 1999.
3. Petsko, G. A.; Ringe, D. *Protein Structure and Function*; New Sciene Press: London, 2004.
4. Liljas, A.; Liljas, L.; Piskur, J.; Lindblom, G.; Nissen, P. *Textbook of Structural Biology*; World Scientific Publishing: Singapore, 2009.
5. Creighton, T. E. *Proteins : Structures and Molecular Properties*; W. H. Freeman and Company: New York, 1993.
6. Barlow, D. J.; Thornton, J. M. Helix Geometry in Proteins. *J. Mol. Biol.* **1988**, *201* (3), 601–619. https://doi.org/10.1016/0022-2836(88)90641-9.
7. Best, R. B.; Buchete, N.-V.; Hummer, G. Are Current Molecular Dynamics Force Fields Too Helical? *Biophys. J.* **2008**, *95* (1), L07–L09. https://doi.org/10.1529/biophysj.108.132696.
8. Best, R. B.; Hummer, G. Optimized Molecular Dynamics Force Fields Applied to the Helix−Coil Transition of Polypeptides. *J. Phys. Chem. B* **2009**, *113* (26), 9004–9015. https://doi.org/10.1021/jp901540t.
9. Piana, S.; Lindorff-Larsen, K.; Shaw, D. E. How Robust Are Protein Folding Simulations with Respect to Force Field Parameterization? *Biophys. J.* **2011**, *100* (9), L47–L49. https://doi.org/10.1016/j.bpj.2011.03.051.
10. Yoda, T.; Sugita, Y.; Okamoto, Y. Comparisons of Force Fields for Proteins by Generalized-Ensemble Simulations. *Chem. Phys. Lett.* **2004**, *386* (4–6), 460–467. https://doi.org/10.1016/j.cplett.2004.01.078.
11. Yoda, T.; Sugita, Y.; Okamoto, Y. Secondary-Structure Preferences of Force Fields for Proteins Evaluated by Generalized-Ensemble Simulations. *Chem. Phys.* **2004**, *307* (2–3), 269–283. https://doi.org/10.1016/j.chemphys.2004.08.002.
12. Cornell, W. D.; Cieplak, P.; Bayly, C. I.; Gould, I. R.; Merz, K. M.; Ferguson, D. M.; Spellmeyer, D. C.; Fox, T.; Caldwell, J. W.; Kollman, P. A. A Second Generation Force Field for the Simulation of Proteins, Nucleic Acids, and Organic Molecules. *J. Am. Chem. Soc.* **1995**, *117* (19), 5179–5197. https://doi.org/10.1021/ja00124a002.
13. Wang, J.; Cieplak, P.; Kollman, P. A. How Well Does a Restrained Electrostatic Potential (RESP) Model Perform in Calculating Conformational Energies of Organic and Biological Molecules? *J. Comput. Chem.* **2000**, *21* (12), 1049–1074. https://doi.org/10.1002/1096-987X(200009)21:12<1049::AID-JCC3>3.0.CO;2-F.
14. Higo, J.; Nishimura, Y.; Nakamura, H. A Free-Energy Landscape for Coupled Folding and Binding of an Intrinsically Disordered Protein in Explicit Solvent from Detailed All-Atom Computations. *J. Am. Chem. Soc.* **2011**, *133* (27), 10448–10458. https://doi.org/10.1021/ja110338e.
15. Chebaro, Y.; Ballard, A. J.; Chakraborty, D.; Wales, D. J. Intrinsically Disordered Energy Landscapes. *Sci. Rep.* **2015**, *5* (1), 10386. https://doi.org/10.1038/srep10386.

16. Shirai, H.; Ikeda, K.; Yamashita, K.; Tsuchiya, Y.; Sarmiento, J.; Liang, S.; Morokata, T.; Mizuguchi, K.; Higo, J.; Standley, D. M.; Nakamura, H. High-Resolution Modeling of Antibody Structures by a Combination of Bioinformatics, Expert Knowledge, and Molecular Simulations. *Proteins Struct. Funct. Bioinforma.* **2014**, *82* (8), 1624–1635. https://doi.org/10.1002/prot.24591.
17. Nishigami, H.; Kamiya, N.; Nakamura, H. Revisiting Antibody Modeling Assessment for CDR-H3 Loop. *Protein Eng. Des. Sel.* **2016**, *29* (11), 477–484. https://doi.org/10.1093/protein/gzw028.
18. Buck, M.; Bouguet-Bonnet, S.; Pastor, R. W.; MacKerell, A. D. Importance of the CMAP Correction to the CHARMM22 Protein Force Field: Dynamics of Hen Lysozyme. *Biophys. J.* **2006**, *90* (4), L36–L38. https://doi.org/10.1529/biophysj.105.078154.
19. Kamiya, N.; Watanabe, Y. S.; Ono, S.; Higo, J. AMBER-Based Hybrid Force Field for Conformational Sampling of Polypeptides. *Chem. Phys. Lett.* **2005**, *401* (1–3), 312–317. https://doi.org/10.1016/j.cplett.2004.11.070.
20. Fujitani, H.; Matsuura, A.; Sakai, S.; Sato, H.; Tanida, Y. High-Level Ab Initio Calculations To Improve Protein Backbone Dihedral Parameters. *J. Chem. Theory Comput.* **2009**, *5* (4), 1155–1165. https://doi.org/10.1021/ct8005437.
21. Robustelli, P.; Piana, S.; Shaw, D. E. Developing a Molecular Dynamics Force Field for Both Folded and Disordered Protein States. *Proc. Natl. Acad. Sci.* **2018**, *115* (21), E4758–E4766. https://doi.org/10.1073/pnas.1800690115.
22. Patel, S.; Brooks, C. L. CHARMM Fluctuating Charge Force Field for Proteins: I Parameterization and Application to Bulk Organic Liquid Simulations. *J. Comput. Chem.* **2004**, *25* (1), 1–16. https://doi.org/10.1002/jcc.10355.
23. Lopes, P. E. M.; Roux, B.; MacKerell, A. D. Molecular Modeling and Dynamics Studies with Explicit Inclusion of Electronic Polarizability: Theory and Applications. *Theor. Chem. Acc.* **2009**, *124* (1–2), 11–28. https://doi.org/10.1007/s00214-009-0617-x.
24. Wieczorek, R.; Dannenberg, J. J. H-Bonding Cooperativity and Energetics of α-Helix Formation of Five 17-Amino Acid Peptides. *J. Am. Chem. Soc.* **2003**, *125* (27), 8124–8129. https://doi.org/10.1021/ja035302q.
25. Wieczorek, R.; Dannenberg, J. J. Hydrogen-Bond Cooperativity, Vibrational Coupling, and Dependence of Helix Stability on Changes in Amino Acid Sequence in Small 3 10 -Helical Peptides. A Density Functional Theory Study. *J. Am. Chem. Soc.* **2003**, *125* (46), 14065–14071. https://doi.org/10.1021/ja034034t.
26. Morozov, A. V.; Tsemekhman, K.; Baker, D. Electron Density Redistribution Accounts for Half the Cooperativity of α Helix Formation. *J. Phys. Chem. B* **2006**, *110* (10), 4503–4505. https://doi.org/10.1021/jp057161f.
27. Wu, Y.-D.; Zhao, Y.-L. A Theoretical Study on the Origin of Cooperativity in the Formation of 3 10 - and α-Helices. *J. Am. Chem. Soc.* **2001**, *123* (22), 5313–5319. https://doi.org/10.1021/ja003482n.
28. Parthasarathi, R.; Raman, S. S.; Subramanian, V.; Ramasami, T. Bader's Electron Density Analysis of Hydrogen Bonding in Secondary Structural Elements of Protein. *J. Phys. Chem. A* **2007**, *111* (30), 7141–7148. https://doi.org/10.1021/jp071513w.
29. Ismer, L.; Ireta, J.; Neugebauer, J. First-Principles Free-Energy Analysis of Helix Stability: The Origin of the Low Entropy in π Helices. *J. Phys. Chem. B* **2008**, *112* (13), 4109–4112. https://doi.org/10.1021/jp077728n.
30. Takano, Y.; Kusaka, A.; Nakamura, H. Density Functional Study of Molecular Interactions in Secondary Structures of Proteins. *Biophys. Physicobiology* **2016**, *13* (0), 27–35. https://doi.org/10.2142/biophysico.13.0_27.
31. Deshmukh, M. M.; Gadre, S. R. Estimation of N−H···O═C Intramolecular Hydrogen Bond Energy in Polypeptides. *J. Phys. Chem. A* **2009**, *113* (27), 7927–7932. https://doi.org/10.1021/jp9031207.
32. Kondo, H. X.; Kusaka, A.; Kitakawa, C. K.; Onari, J.; Yamanaka, S.; Nakamura, H.; Takano, Y. Hydrogen Bond Donors and Acceptors Are Generally Depolarized in α-Helices as Revealed by a Molecular Tailoring Approach. *J. Comput. Chem.* **2019**, *40* (23), 2043–2052. https://doi.org/10.1002/jcc.25859.
33. Frisch, M. J.; Trucks, G. W.; Schlegel, H. B.; Scuseria, G. E.; Robb, M. A.; Cheeseman, J. R.; Scalmani, G.; Barone, V.; Mennucci, B.; Petersson, G. A.; Nakatsuji, H.; Caricato, M.; Li, X.; Hratchian, H. P.; Izmaylov, A. F.; Bloino, J.; Zheng, G.; Sonnenberg, J. L.; Hada, M.; Ehara, M.; Toyota, K.; Fukuda, R.; Hasegawa, J.; Ishida, M.; Nakajima, T.; Honda, Y.; Kitao, O.; Nakai, H.; Vreven, T.; Montgomery Jr., J. A.; Peralta, J. E.; Ogliaro, F.; Bearpark, M.; Heyd, J. J.; Brothers, E.; Kudin, K. N.; Staroverov, V. N.; Kobayashi, R.; Normand, J.; Raghavachari, K.; Rendell, A.; Burant, J. C.; Iyengar, S. S.; Tomasi, J.; Cossi, M.; Rega, N.; Millam, J. M.; Klene, M.; Knox, J. E.; Cross, J. B.; Bakken, V.; Adamo, C.; Jaramillo, J.; Gomperts, R.; Stratmann, R. E.; Yazyev, O.; Austin, A. J.; Cammi, R.; Pomelli, C.; Ochterski, J. W.; Martin, R. L.; Morokuma, K.; Zakrzewski, V. G.; Voth, G. A.; Salvador, P.; Dannenberg, J. J.; Dapprich, S.; Daniels, A. D.; Farkas, Ö.; Foresman, J. B.; Ortiz, J. V; Cioslowski, J.; Fox, D. J. Gaussian 09, Revision C.01. *Gaussian Inc Wallingford CT*. 2009, p Wallingford CT. https://doi.org/10.1159/000348293.
34. Pettersen, E. F.; Goddard, T. D.; Huang, C. C.; Couch, G. S.; Greenblatt, D. M.; Meng, E. C.; Ferrin, T. E. UCSF Chimera?A Visualization System for Exploratory Research and Analysis. *J. Comput. Chem.* **2004**, *25* (13), 1605–1612. https://doi.org/10.1002/jcc.20084.
35. Humphrey, W.; Dalke, A.; Schulten, K. VMD: Visual Molecular Dynamics. *J. Mol. Graph.* **1996**, *14* (1), 33–38. https://doi.org/10.1016/0263-7855(96)00018-5.
36. Cieplak, P.; Cornell, W. D.; Bayly, C.; Kollman, P. A. Application of the Multimolecule and Multiconformational RESP Methodology to Biopolymers: Charge Derivation for DNA, RNA, and Proteins. *J. Comput. Chem.* **1995**, *16* (11), 1357–1377. https://doi.org/10.1002/jcc.540161106.